Geophysical Research Letters

RESEARCH LETTER
10.1029/2020GL088036

Mechanisms Underlying Recent Arctic Atlantification

Helene Asbjørnsen[1,2], Marius Årthun[1,2], Øystein Skagseth[2,3], and Tor Eldevik[1,2]

[1]Geophysical Institute, University of Bergen, Bergen, Norway, [2]Bjerknes Centre for Climate Research, Bergen, Norway, [3]Institute of Marine Research, Bergen, Norway

Key Points:
- Atlantification of the Barents Sea and Fram Strait is documented using the ECCOv4-r3 ocean state estimate
- Mechanisms driving the warming trends along Atlantic water pathways are regionally dependent and not stationary in time
- Stratification is weakened in the northern Barents Sea, but increased vertical temperature fluxes are not driving the upper-ocean warming

Supporting Information:
- Supporting Information S1

Correspondence to:
H. Asbjørnsen,
H.Asbjornsen@uib.no

Citation:
Asbjørnsen H., Årthun, M., Skagseth, Ø., & Eldevik, T. (2020). Mechanisms underlying recent Arctic Atlantification. *Geophysical Research Letters*, *47*, e2020GL088036. https://doi.org/10.1029/2020GL088036

Received 9 APR 2020
Accepted 4 JUN 2020
Accepted article online 20 JUN 2020

Abstract Recent warming and reduced sea ice concentrations in the Atlantic sector of the Arctic Ocean are the main signatures of ongoing Arctic "Atlantification." The mechanisms driving the warming trends are nevertheless still debated, particularly regarding the relative importance of oceanic and atmospheric heat fluxes. Here, heat budgets along main Atlantic water pathways through the Barents Sea and Fram Strait are constructed to investigate the mechanisms of Atlantification during 1993–2014. The largest warming trends occur south of the winter ice edge, with ocean advection as the main driver. Warming in the marginal ice zone is mainly due to low surface heat loss from the 1990s to the mid-2000s. In the ice-covered northwestern Barents Sea, ocean advection and air-sea heat fluxes act in concert to drive a gradual warming of the upper ocean. Despite a weakened stratification, no evidence is found of vertical oceanic temperature fluxes driving this upper-ocean warming.

Plain Language Summary Recent "Atlantification" of the Arctic is characterized by warmer ocean temperatures and a reduced sea ice cover. The Barents Sea is a "hot spot" for these changes, something which has broad socioeconomic and environmental impacts in the region. However, there is, at present, no complete understanding of what is causing the ocean warming. Here, we determine the relative importance of transport of heat by ocean currents (ocean advection) and heat exchanges between the atmosphere and the ocean (air-sea heat fluxes) in warming the Barents Sea and Fram Strait. In the ice-free region, ocean advection is found to be the main driver of the warming trend due to increasing inflow temperatures between 1996 and 2006. In the marginal ice zone and the ice-covered northern Barents Sea, ocean advection and air-sea heat fluxes are found to be of interchanging importance in driving the warming trend through the 1993–2014 period analyzed. A better understanding of the recent warming trends in the Barents Sea and Fram Strait has implications for how we understand the ocean's role in ongoing and future Arctic climate change.

1. Introduction

The Arctic is currently experiencing rapid climate change manifested in the ocean and cryosphere (Carmack et al., 2015), as well as in the atmosphere and on land (Elmendorf et al., 2012; Kohnemann et al., 2017). The Barents Sea is a "hot spot" for Arctic climate change (Lind et al., 2018; Schlichtholz, 2019; Skagseth et al., 2020), with pronounced upper-ocean warming and a retreating sea ice cover over the past two decades (Figures 1a and 1b). Associated changes to the surface energy budget have implications for atmospheric circulation patterns, with potential impacts outside the immediate Arctic climate system (e.g., Screen et al., 2018; Sorokina et al., 2016). Additionally, the changing environmental conditions in the region alter distribution and migration patterns of local fish communities (Fossheim et al., 2015) and reduces the habitats of ice-dependent mammals (Descamps et al., 2017).

The Barents Sea is a shallow shelf sea in the Atlantic sector of the Arctic Ocean. With a seasonal ice cover, the sea ice reaches its maximum extent in March/April and minimum in September (Signorini & McClain, 2009). Warm and saline Atlantic water enters the western Barents Sea through the Barents Sea Opening (BSO) and flows northward following two main pathways—one going east into the Central Basin before turning north and eventually exiting through the St. Anna Trough and one shorter pathway turning north along the Hopen Trench (Loeng, 1991). Additionally, the West Spitsbergen Current transports Atlantic water poleward through the Fram Strait along the west coast of Svalbard (Aagaard et al., 1987). Considerable cooling and freshening occur along these pathways—cooling in the ice-free region where the water column loses heat to the Arctic atmosphere and freshening when the Atlantic water meets the fresh surface layer in the marginal ice zone (Smedsrud et al., 2010).

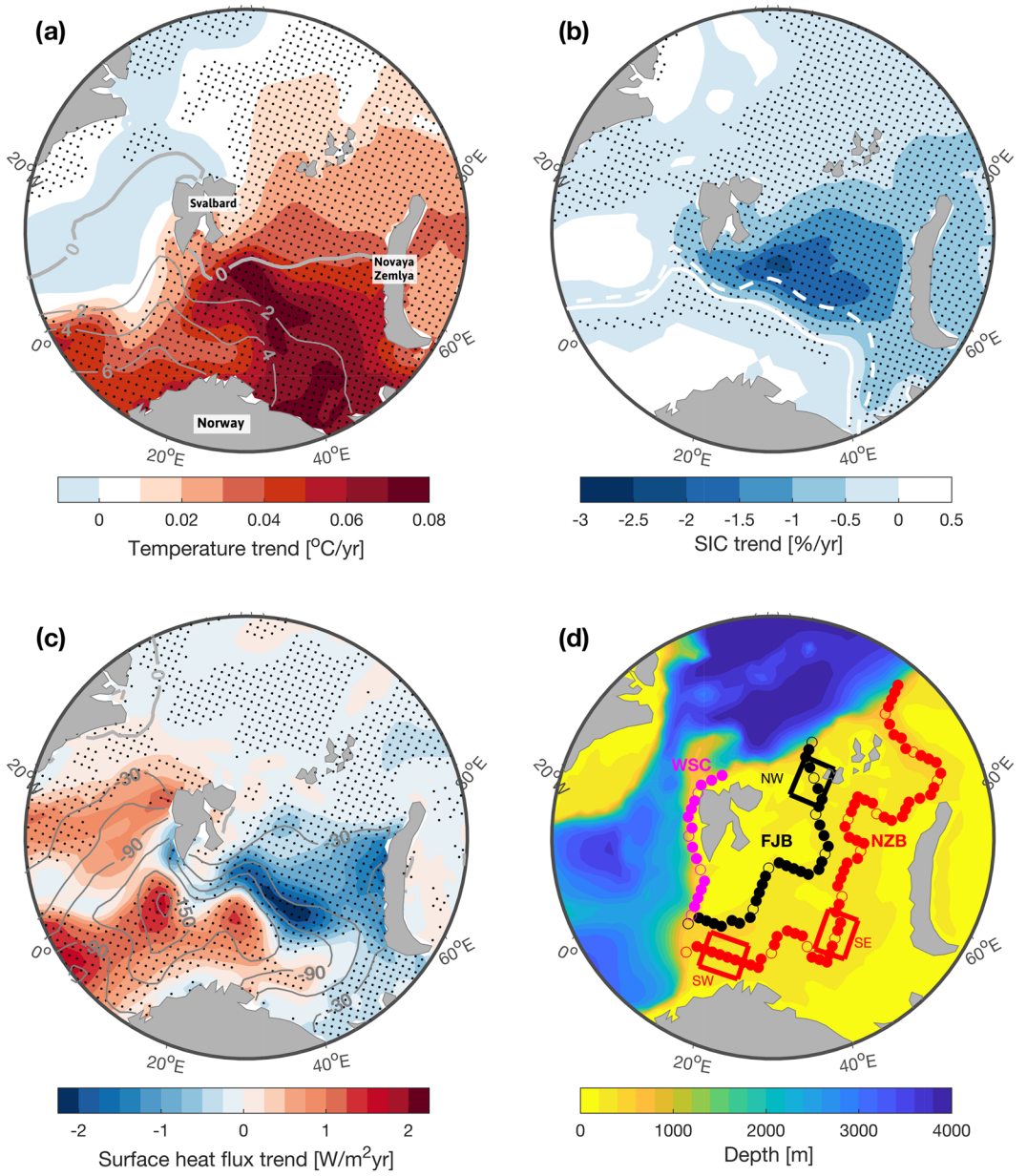

Figure 1. Linear trends over the 1993–2014 period. (a) Upper-ocean (0–100 m) temperature trend (shadings) with time mean temperature (gray contour lines: −2:2:6°C). (b) Sea ice concentration trend (shadings) with mean April ice edge (15% SIC) for 1993–2003 (solid white line) and 2004–2014 (dashed white line). (c) Net surface heat flux trend (shadings) with time mean net surface heat flux (gray contour lines: −180:30:0 W/m^2). Negative trend value indicates increased ocean heat loss (ocean cooling); positive trend value indicates reduced ocean heat loss (ocean warming). (d) Bathymetry, Atlantic water pathways, and regions defined for the heat budget analysis: Novaya Zemlya branch (NZB; red), Franz Josef branch (FJB; black), West Spitsbergen Current (WSC; magenta), southwestern box (SW), southeastern box (SE), and northwestern box (NW). Every 200 km has an open marker. Dots in (a)–(c) indicate where the trends are significant at the 95% confidence level.

With recent warming of the Atlantic water inflow and coinciding retreat of the ice cover, the increased influence of Atlantic water in the region has been termed an "Atlantification" of the Arctic Ocean (Årthun et al., 2012; Polyakov et al., 2017). This definition of Atlantification includes both Atlantic water extending further poleward and/or occupying a larger part of the water column—both resulting in a warming and salinification of the region. Different mechanisms have, however, been proposed explaining such Atlantification, and their relative importance in the overall warming of the Arctic Ocean is still debated. Changes in the strength

and properties of the inflowing Atlantic water have been shown to affect winter sea ice growth and consequently the size of the ice-free "Atlantic domain" in the Barents Sea (Årthun et al., 2012; Sandø et al., 2010). Changes in stratification, leading to an increased vertical oceanic heat flux from the submerged Atlantic water layer, have been proposed as an important mechanism for upper-ocean warming in the northwestern Barents Sea (Lind et al., 2018) and the Eurasian Basin of the Arctic Ocean (Polyakov et al., 2017). Additionally, changes in the atmospheric circulation can create oceanic heat anomalies through changes in local air-sea heat fluxes (Kim et al., 2019; Woods & Caballero, 2016).

To identify the mechanisms underlying recent Arctic Atlantification, we here present a first detailed spatio-temporal heat budget along the main poleward pathways of Atlantic water. We use the ECCO Version 4 Release 3 (referred to as ECCOv4-r3) ocean state estimate (Forget, Campin, et al., 2015; Fukumori et al., 2017), ideal for heat budget analysis due to its closed heat budget diagnostics (Asbjørnsen et al., 2019; Buckley et al., 2015; Foukal & Lozier, 2018; Piecuch et al., 2017). By quantifying the contribution of air-sea heat fluxes, and vertical and horizontal advective and diffusive oceanic temperature fluxes, we explore Barents Sea and Fram Strait warming trends in recent decades.

2. Methods

ECCOv4-r3 is an ocean state estimate of the 1992–2015 global ocean circulation and sea ice state, with a 1° nominal horizontal resolution (Forget, Campin, et al., 2015; Fukumori et al., 2017). The grid spacing in the Barents Sea region is roughly 45 km. The state estimate is generated by the ice-ocean component of the Massachusetts Institute of Technology general circulation model (MITgcm) solving the primitive equations for a time-evolving, Boussinesq, hydrostatic ocean, with solutions fitted to satellite and in situ ocean observations through the adjoint method (Heimbach et al., 2005). ERA-Interim reanalysis (Dee et al., 2011) is used as the initial near surface atmospheric state (air temperature, humidity, precipitation, downward radiation, and wind stress), while air-sea heat fluxes are calculated from bulk formulae (Large & Yeager, 2004). The long-term (1992–2015) mean turbulent heat fluxes calculated within the ECCOv4-r3 framework are consistent with ERA-Interim in both the southern (71–73°N, 20–30°E; −109 and −102 W/m^2, respectively) and northern Barents Sea (77–80°N, 30–40°E; −21 W/m^2 for both), and the interannual variability is similar ($r_{south} = 0.75$ and $r_{north} = 0.45$). The effect of unresolved eddies is parameterized as a bolus velocity (Gent & Mcwilliams, 1990). Turbulent transport parameters, such as the Gent-McWilliams bolus velocity (eddy) coefficient, are estimated within the ECCOv4-r3 framework under the constraints of observations (Forget, Campin, et al., 2015), something which greatly improves the fit to in situ profiles compared to earlier ECCO solutions (Forget, Ferreira, et al., 2015). The ECCOv4-r3 state estimate ensures closed heat, salt, and volume budgets, as the adjoint method avoids adding nonphysical source/sink terms to the model equations when constraining to observations.

The ECCOv4-r3 estimate reproduces well observed Atlantic water properties in the Nordic and Barents seas (Asbjørnsen et al., 2019; Carton et al., 2019), including temperature trends and variability in the BSO and Kola sections (supporting information Figure S2; $r_{BSO} = 0.89$ and $r_{Kola} = 0.93$). These are regions with relatively high observational data coverage (Figure S1), contributing to a well-constrained state estimate. Observations over the water column are fewer in the ice-covered regions, and satellite observations of sea ice concentration (SIC) therefore becomes a valuable constraint. Correct seasonal and interannual variability in the ice cover is, for instance, crucial for simulating stratification changes (e.g., Ellingsen et al., 2009). The comparison between observed and ECCOv4-r3 summer stratification in the northwestern Barents Sea (77–80°N, 30–40°E) is encouraging (Figure S3), with ECCOv4-r3 simulating the main features of the observed water masses: a warm and fresh surface layer, a cold and fresh Arctic layer, and a warm and saline Atlantic water layer at depth. ECCOv4-r3 nevertheless appears to be less stratified in both temperature and salinity compared to observations. However, as in observations (Figures S3a and S3b), a thinning Arctic layer is found during the 2000s (Figures S3c and S3d), in addition to a distinct surface warming and salinification over the 1993–2014 period.

The three Atlantic water pathways in Figure 1d are defined according to time mean barotropic stream function contours in ECCOv4-r3 and found to be consistent with the circulation patterns known from observations (e.g., Loeng, 1991). Following Aksenov et al. (2010), the three pathways will be referred to as the Novaya Zemlya branch (NZB), the Franz Josef branch (FJB), and the West Spitsbergen Current (WSC).

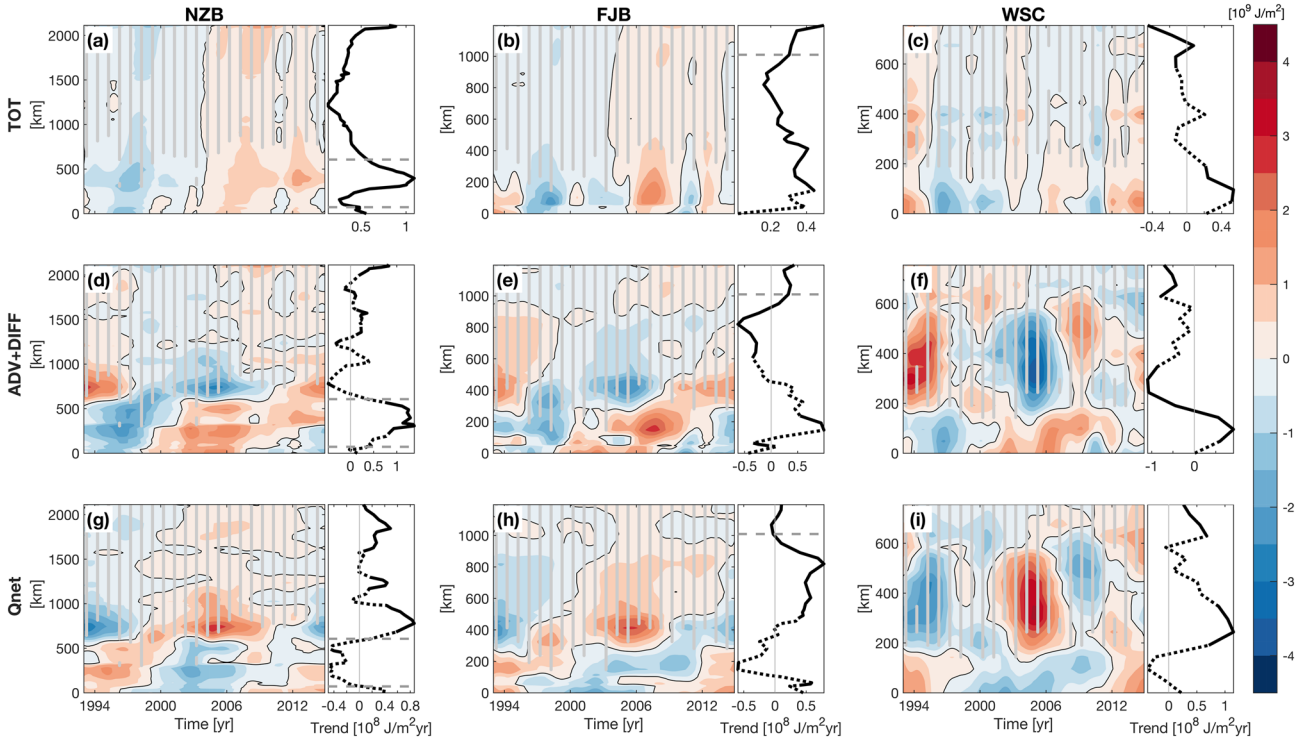

Figure 2. Along-path heat budget (full depth). (a–c) Heat content anomaly (per square meter) *TOT*. (d–f) Combined effect of advective and diffusive heat transport convergences *ADV+DIFF*. (g–i) Net air-sea heat fluxes *Qnet*. (a–i) Corresponding linear trend over the 1993–2014 period in black lines (dashed when not significant at the 95% confidence level). The center of the three boxes in Figure 1d is marked with gray horizontal dashed lines. Gray vertical lines mark areas with April sea ice concentrations higher than 15%. Note different scales on the *y* axes for the different pathways.

Start and end points of the pathways are chosen according to where the stream function contours come onto and off the continental shelf. Additionally, three boxes are defined in order to capture different regimes in the Barents Sea. The Southwestern box (SW) is located along the NZB and captures the ice-free Atlantic water inflow region. The Southeastern box (SE) is also located along the NZB but in the marginal ice zone. Finally, the Northwestern box captures the ice-covered northwest along the FJB.

The heat budget in J/m^2 is calculated by integrating the conservation of heat equation in time and depth z:

$$\underbrace{\rho_o C_p \int_t \int_z \frac{\partial \theta}{\partial t}\, dz\, dt}_{TOT} = \underbrace{\rho_o C_p \int_t \int_z \left(-\Delta \cdot \mathbf{u}\theta - \frac{\partial (w\theta)}{\partial z}\right) dz\, dt}_{ADV} + \underbrace{\rho_o C_p \int_t \int_z (-\Delta \cdot \mathbf{K})\, dz\, dt}_{DIFF} + \underbrace{\rho_o C_p \int_t \int_z Q\, dz\, dt}_{Qnet}, \quad (1)$$

where ρ_o is a reference density of seawater, C_P is the specific heat capacity, θ is potential temperature, $\mathbf{u}$ is the horizontal velocity vector, w is the vertical velocity, $\mathbf{K}$ is the three-dimensional diffusive temperature flux vector in °C m/s (from diapycnal diffusion and parameterized isopycnal diffusion), and Q is the net air-sea temperature flux in °C/s. For simplicity, the budget terms are referred to as total heat content *TOT*, advective heat transport convergence *ADV*, diffusive heat transport convergence *DIFF*, and net air-sea heat fluxes *Qnet*. The vertically integrated heat budgets displayed are time anomaly budgets, meaning that the time mean has been removed from each budget term in each horizontal grid cell after the depth integration. This implies that all budget results are relative to the mean rates of change over the study period. However, ocean heat content calculated directly from temperature shows practically the same trends and variability as *TOT* (not shown), and our interpretation and discussion of ocean heat content change and its drivers are therefore not impacted by the specific method of budget calculation used here. The along-path heat budgets (Figure 2) are integrated from the sea surface to the ocean bottom to focus on the relative roles of oceanic (*ADV+DIFF*) and atmospheric (*Qnet*) forcing on the water

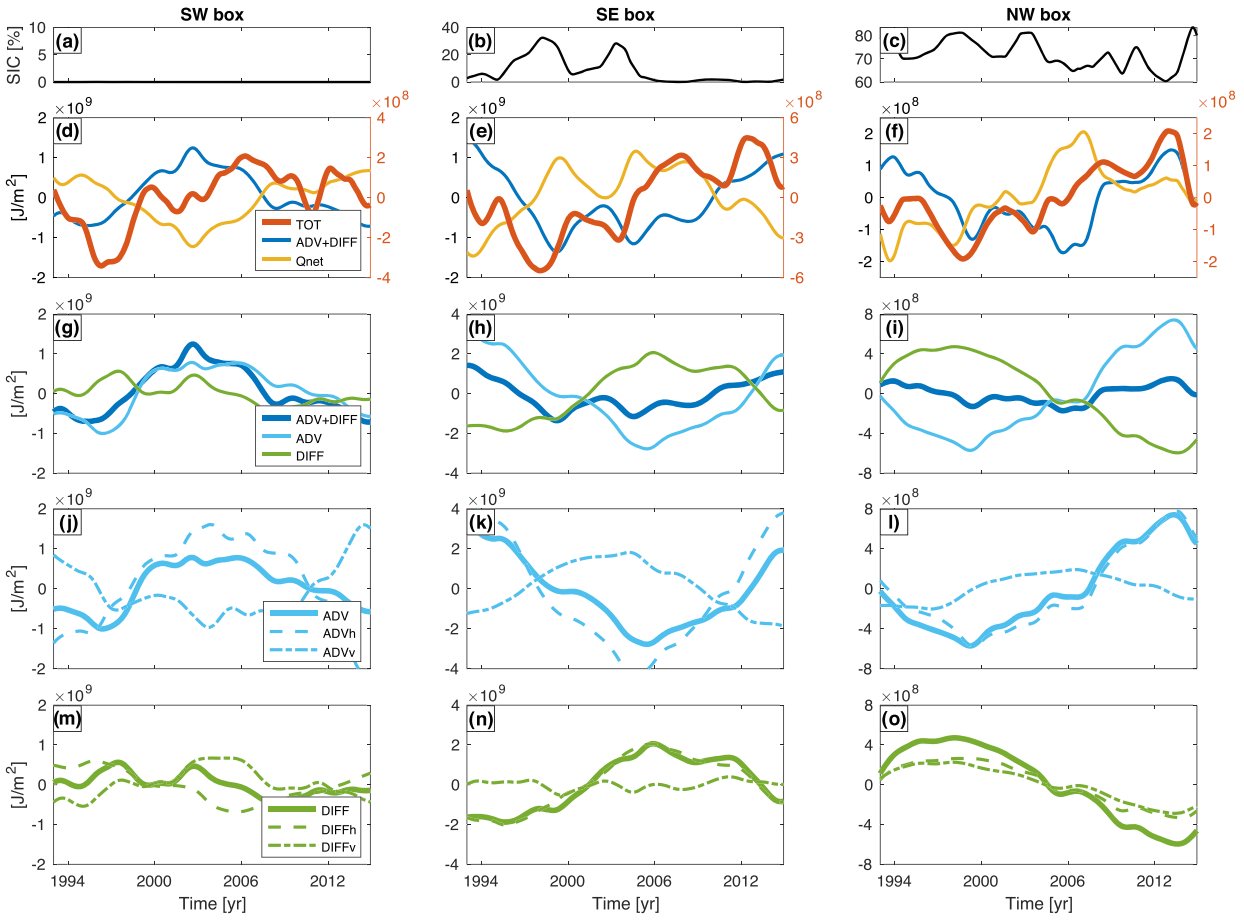

Figure 3. Upper-ocean heat budgets. (a–c) Sea ice concentration evolution in time, averaged over boxes in Figure 1d. (d–i) Heat budget (0–100 m) for boxes, with decomposition of advective heat transport convergence *ADV* (j–l) and diffusive heat transport convergence *DIFF* (m–o) into horizontal and vertical contributions. Note different scales on the *y* axes.

column, while the box heat budgets (Figure 3) are integrated over the upper 100 m in order to explore the effect of vertical advective heat transport in recent upper-ocean warming.

When diagnosing horizontal and vertical advection and diffusion (Figure 3), it is important to note that these are "temperature fluxes" relative to an arbitrary reference temperature, as the condition of zero net volume transport is not necessarily met. Here, we use 0°C as commonly used for the Barents Sea (Smedsrud et al., 2013; Wang et al., 2019). We have also calculated the temperature fluxes using the time-evolving volume-weighted temperature for the three boxes as reference temperature (Lee et al., 2004) and find that the relative contributions to *TOT* are largely unchanged.

All time series are smoothed by applying a 1-year low-pass triangular filter (24-month filter width), as we focus on interannual variability and change. The first and last 12 months of the 1992–2015 time series are removed to avoid edge effects from filtering, leaving us with the 1993–2014 time period analyzed here. Linear trends over the 1993–2014 period are calculated using the least squares method, and significance tested (95% confidence) with the modified Mann-Kendall trend test for autocorrelated data (Hamed & Rao, 1997).

3. Results and Discussion

For the Atlantic water pathways through the Barents Sea (NZB and FJB), a net warming of the water column is found along the entire pathway (Figures 2a and 2b). For the pathway through the Fram Strait (WSC), an overall warming trend is also seen in the southernmost part, although significant for only a limited part of

the pathway (Figure 2c). In the following sections we discuss the dominant mechanisms driving the warming along the three pathways according to three dynamically distinct regions: the open ocean, the marginal ice zone, and the ice-covered ocean.

3.1. Open Ocean

Because of the warm Atlantic water inflow through the BSO, the southwestern Barents Sea is ice-free, also in winter (Årthun et al., 2012; Loeng, 1991). It is also in this region the ocean climatologically loses the most heat to the Arctic atmosphere (Figure 1c), which is colder than the ocean most of the year (Smedsrud et al., 2010).

The open ocean domain is represented by the southernmost parts of the three Atlantic water pathways (Figure 2; 0–500 km along NZB, 0–250 km along FJB, and 0–150 km along WSC) and the SW box in Figure 3. As seen in Figures 2a–2c, the largest warming trends over the 1993–2014 period are found in this open ocean region. Advective and diffusive heat transport convergences (*ADV* + *DIFF*) in the 1990s and early 2000s are the main source of the overall warming (Figures 2d–2f), with an additional warming contribution from surface heat fluxes (*Qnet*) from the mid-2000s to the end of the period (Figures 2g–2i). For instance, in the open ocean domain along the NZB the mean cooling trend by *Qnet* is 23% of the mean warming trend by *ADV* + *DIFF*. The temporal evolution of the budget terms for the upper ocean (0–100 m; Figure 3) furthermore demonstrates that horizontal temperature flux convergence (*ADVh*) is the main contributor to changes in *ADV*+*DIFF* (Figures 3g and 3j; $r(ADVh, ADV + DIFF) = 0.86$). It is worth noting that *Qnet* and *ADV* + *DIFF* are strongly anticorrelated, and of opposing trends, in the open ocean domain (e.g., Figure 3d; $r = -0.97$). Often the large, but competing, budget terms leave a comparatively small heat content change. The competing budget terms reflect the opposing and close link between anomalous Atlantic heat transport and surface heat fluxes in the southern Barents Sea (Sandø et al., 2010; Smedsrud et al., 2010); for example, a warming by *ADV*+*DIFF* is followed by elevated heat loss to the atmosphere, which will be expressed in the heat budget as cooling by *Qnet*.

Horizontal advection of heat being an important driver in warming the southwestern Barents Sea is consistent with the traditional view of Atlantification by increased heat transport through the BSO (Årthun et al., 2012; Koenigk & Brodeau, 2014; Sandø et al., 2010). From observations, temperatures in the BSO have increased in recent decades, with a particular steep warming trend between 1996 and 2006 (Figure S2a). This period of enhanced warming in the BSO fits well with the period where warming of the open ocean domain in Figures 2d–2f is driven by *ADV* + *DIFF*. In a recent ocean-ice hindcast simulation the long-term trend in heat transport through the BSO is found to mainly stem from increasing ocean temperatures in the subpolar North Atlantic (Wang et al., 2019) and thus further connecting the warming of the southwestern Barents Sea to warm anomalies upstream.

Despite the Barents Sea being in a warm state, our results show a reduced ocean heat loss in the open ocean domain in recent years (Figure 1c). This particular mechanism has been highlighted in previous studies, connecting reduced regional heat loss since the mid-2000s to more southwesterly winds and consequently a warmer and more humid atmosphere (Skagseth et al., 2020; Woods & Caballero, 2016). Our heat budget confirms that reduced ocean heat loss contributes to the accumulated heat content anomaly since the mid-2000s (Figure 3d).

3.2. Marginal Ice Zone

The marginal ice zone is the transition between the open ocean and the ice-covered ocean. While there is large interannual variability in the Barents Sea ice extent and therefore the exact location of the marginal ice zone, the negative trend in SIC has led to an overall northward retreat of the ice edge (Figure 1b). As a result, the area in the vicinity of the ice edge has experienced an elevated ocean heat loss in recent years (Figure 1c).

Heat budgets from the marginal ice zone are here represented by the part of the three pathways in the proximity of the sea ice edge (Figure 2; 500–900 km along NZB, 250–500 km along FJB, and 150–400 km along WSC) and by the SE box in Figure 3. In the Barents Sea, a warming contribution from *Qnet* from the 1990s to the mid-2000s, together with a warming contribution from *ADV* + *DIFF* from the mid-2000s to the end of the period, explain the overall warming trend in the marginal ice zone. For the WSC pathway through the Fram Strait, *Qnet* also gives a warming contribution from the 1990s to the mid-2000s, but

opposing trends in *ADV+DIFF* compensate to the extent that the overall warming trend in Figure 2c is not significant in this region.

In the marginal ice zone, the trend and variability in ocean heat content is intrinsically linked to the trend and variability in the sea ice cover. The onset of the cooling contribution from *Qnet* in the southeastern Barents Sea during 2005–2014 (Figure 3e) notably coincides with the region becoming practically ice-free after 2005 (Figure 3b). The warming contribution from ADV+DIFF during the same period is due to gradually increasing temperatures of the inflowing water at the southwestern boundaries between 1998 and 2012, and the cold Arctic layer retreating out of the box as sea ice is retreating. This is consistent with the understanding of the Barents Sea as a "cooling machine," with higher ocean temperatures being damped by an increase in the open ocean area (less sea ice) and larger oceanic heat loss (Årthun et al., 2012; Smedsrud et al., 2013). However, this damping effect of the "cooling machine" has been called into question, as additional heat loss from sea ice loss will be marginal when the Barents Sea becomes increasingly ice-free in winter (Skagseth et al., 2020).

3.3. Ice-Covered Ocean

The northern Barents Sea has an Arctic climate and is ice-covered for most of the year. The hydrography is characterized by cold, fresh Arctic waters sitting on top of modified Atlantic water (e.g., Lind et al., 2018; Loeng, 1991). Although the Atlantic water is not in direct contact with the surface, also this region has experienced a warming of the upper ocean and reduced SICs over the 1993–2014 period (Figures 1a and 1b).

To assess the mechanisms responsible for warming the northern Barents Sea, we investigate heat budgets along the northernmost parts of the three pathways (Figure 2; north of 900 km along NZB, north of 500 km along FJB, and north of 400 km WSC) and for the NW box (Figure 3). The overall warming trend along NZB and FJB is in general weaker in the ice-covered domain than in the open ocean and the marginal ice zone (Figures 2a and 2b)—the very northernmost part of the pathways close to the shelf break being an exception. In contrast to the open ocean and marginal ice zone, oceanic and atmospheric forcing in the ice-covered domain are found to act in concert to drive the overall warming of the water column (Figures 2d, 2e, 2g, and 2h) and the upper ocean (Figure 3f; $r(TOT,ADV+DIFF)=0.49$, $r(TOT,Qnet)=0.56$). This regionally different behavior could result from the isolating effect of the seasonal ice cover and the more stratified water column in the northern Barents Sea, decoupling subsurface heat content anomalies from the atmosphere.

Although the Arctic layer in the northwestern Barents Sea is found to be thinning toward the end of the 1993–2014 period (Figures S3c and S3d), leading to reduced upper-ocean stratification, we find no evidence of vertical temperature fluxes from the underlying Atlantic water layer driving the upper-ocean warming (Figure 3l). Instead, horizontal temperature flux convergence (*ADVh*) largely determines changes in *ADV+DIFF* ($r = 0.64$), as for the ice-free SW box and the SE box in the marginal ice zone. For the NW box, the warming trend in *ADVh* between 1999 and 2013 is specifically explained by increasing temperatures of the inflowing water from the south and a reduced throughflow after 2006 (i.e., weaker transport of water with subzero temperatures).

Our results show an upper-ocean warming of the northern Barents Sea in line with Lind et al. (2018). However, in contrast to what is hypothesized in Lind et al. (2018), the heat budget analysis does not point to enhanced vertical mixing and increased upward fluxes as the source of the warming. We do interestingly find positive trends in vertical velocities over the 1993–2014 period in winter (Figure S4). The same dominance of *ADVh* is, however, found in January budgets as well as in August budgets for the NW box and for the larger 77–80°N, 30–40°E box (not shown). We therefore conclude that within the ECCOv4-r3 framework, vertical processes have not been a main driver of the upper-ocean warming of the Barents Sea. It is worth noting that the coarse vertical resolution (50 unevenly spaced vertical levels) means that processes related to vertical mixing are largely parameterized, and vertical transport of heat could therefore be underrepresented. However, in contrast to commonly used ocean reanalysis products, ECCOv4-r3 ensures vertical velocities and fluxes that are dynamically and kinematically consistent while constrained to available observational data (Forget, Ferreira, et al., 2015; Liang et al., 2017).

4. Summary and Conclusions

The Arctic Ocean has warmed significantly in recent decades (Figure 1a). During the 1993–2014 period analyzed here, the Barents Sea transitioned to a warmer state, with reduced SICs and Atlantic water extending further poleward in the latter half of the period compared to the first half of the period (Figures 1a and 1b). The mechanisms underlying this Atlantification have been investigated by constructing spatiotemporal heat budgets for three main Atlantic water pathways toward the Arctic Ocean basin. For the Atlantic water pathways through the Barents Sea, a significant warming of the water column is identified along the entire pathway (Figures 2a and 2b). The warming trend in the Fram Strait is, on the other hand, much less distinct and in general not significant (Figure 2c).

The heat budgets presented here reveal a complex Arctic climate system where the underlying mechanisms driving the recent Atlantification are found to be regionally dependent and not stationary in time. While the warming of the southern Barents Sea is largely due to a warming of the Atlantic water inflow between 1996 and 2006 (Figure 2a), reduced ocean heat loss to the atmosphere has also contributed to the warming trend toward the end of the 1993–2014 period. We find no evidence of vertical oceanic temperature fluxes driving the upper-ocean warming of the northwestern Barents Sea. However, increasing vertical velocities in winter over the 1993–2014 period are identified (Figure S4), which could suggest an increasingly important role for vertical oceanic temperature fluxes in the future, as the stratification is likely to weaken when the Barents Sea becomes increasingly ice-free (Onarheim & Årthun, 2017).

In this study we have focused on interannual variability and trends in ocean heat content. Seasonal variability in the Barents Sea is pronounced, for example, in Atlantic heat transport (Årthun et al., 2012), surface heat fluxes (Smedsrud et al., 2010), and sea ice cover (Signorini & McClain, 2009), and the annual budgets and associated mechanisms presented here represent the combined effect of different processes acting in different seasons. The upper-ocean warming in recent decades is nevertheless of similar magnitude in all seasons (not shown), consistent with winter temperatures determining the temperature in the Barents Sea for the rest of the year (Ottersen et al., 2000).

By presenting the first spatiotemporal heat budget for the Barents Sea and Fram Strait, our study has identified regionally different mechanisms underlying recent warming trends and thus contributes to bridge the gap and resolve previously divergent findings. As Atlantification is projected to move northeastward along the Atlantic water pathways in the future (Årthun et al., 2019), a better understanding of recent warming trends in the Barents Sea and Fram Strait has implications for how we understand the ocean's role in ongoing and future Arctic climate change.

Data Availability Statement

The ECCOv4-r3 ocean state estimate is available online (at https://ecco.jpl.nasa.gov/drive/files/Version4/Release3/). ERA-Interim reanalysis is available online (athttps://www.ecmwf.int/en/forecasts/datasets/archive-datasets/reanalysis-datasets/era-interim/). Time series of BSO and Kola temperatures are available online (at https://ocean.ices.dk/iroc/).

Acknowledgments

This study was funded by the Research Council of Norway projects PATHWAY (Grant 263223) and Nansen Legacy (Grant 276730), the Blue-Action project (European Union's Horizon 2020 research and innovation program; Grant 727852), and the Trond Mohn Foundation (Grant BFS2018TMT01). The authors thank Christopher Piecuch and one anonymous reviewer for their constructive comments that improved the manuscript.

References

Aagaard, K., Foldvik, A., & Hillman, S. R. (1987). The West Spitsbergen Current: Disposition and water mass transformation. *Journal of Geophysical Research*, *92*(C4), 3778–3784. https://doi.org/10.1029/JC092iC04p03778

Aksenov, Y., Bacon, S., Coward, A. C., & Nurser, A. J. G. (2010). The North Atlantic inflow to the Arctic Ocean: High-resolution model study. *Journal of Marine Systems*, *79*(1-2), 1–22. https://doi.org/10.1016/J.JMARSYS.2009.05.003

Årthun, M., Eldevik, T., & Smedsrud, L. H. (2019). The role of Atlantic heat transport in future Arctic winter sea ice loss. *Journal of Climate*, *32*, 3327–3341. https://doi.org/10.1175/JCLI-D-18-0750.1

Årthun, M., Eldevik, T., Smedsrud, L. H., Skagseth, O., & Ingvaldsen, R. B. (2012). Quantifying the influence of Atlantic heat on Barents Sea ice variability and retreat. *Journal of Climate*, *25*(13), 4736–4743. https://doi.org/10.1175/JCLI-D-11-00466.1

Asbjørnsen, H., Årthun, M., Skagseth, O., & Eldevik, T. (2019). Mechanisms of ocean heat anomalies in the Norwegian Sea. *Journal of Geophysical Research: Oceans*, *124*, 2908–2923. https://doi.org/10.1029/2018JC014649

Buckley, M. W., Ponte, R. M., Forget, G., & Heimbach, P. (2015). Determining the origins of advective heat transport convergence variability in the North Atlantic. *Journal of Climate*, *28*(10), 3943–3956. https://doi.org/10.1175/JCLI-D-14-00579.1

Carmack, E., Polyakov, I., Fer, I., Hunke, E., Hutchings, J., Jackson, J., et al. (2015). Toward quantifying the increasing role of oceanic heat in sea ice loss in the new Arctic. *Bulletin of the American Meteorological Society*, *96*(12), 2079–2105. https://doi.org/10.1175/BAMS-D-13-00177.1

Carton, J. A., Penny, S. G., & Kalnay, E. (2019). Temperature and salinity variability in the SODA3, ECCO4r3, and ORAS5 ocean reanalyses, 1993-2015. *Journal of Climate*, *32*(2), 2277–2293. https://doi.org/10.1175/JCLI-D-18-0605.1

Dee, D. P., Uppala, S. M., Simmons, A. J., Berrisford, P., Poli, P., Kobayashi, S., et al. (2011). The ERA-Interim reanalysis: Configuration and performance of the data assimilation system. *Quarterly Journal of the Royal Meteorological Society*, *137*(656), 553–597. https://doi.org/10.1002/qj.828

Descamps, S., Aars, J., Fuglei, E., Kovacs, K. M., Lydersen, C., Pavlova, O., et al. (2017). Climate change impacts on wildlife in a High Arctic archipelago—Svalbard, Norway. *Global Change Biology*, *23*(2), 490–502. https://doi.org/10.1111/gcb.13381

Ellingsen, I., Slagstad, D., & Sundfjord, A. (2009). Modification of water masses in the Barents Sea and its coupling to ice dynamics: A model study. *Ocean Dynamics*, *59*(6), 1095–1108. https://doi.org/10.1007/s10236-009-0230-5

Elmendorf, S. C., Henry, G. H. R., & Hollister, R. D. (2012). Plot-scale evidence of tundra vegetation change and links to recent summer warming. *Nature Climate Change*, *2*, 453–457. https://doi.org/10.1038/NCLIMATE1465

Forget, G., Campin, J.-M., Heimbach, P., Hill, C. N., Ponte, R. M., & Wunsch, C. (2015). ECCO version 4: An integrated framework for non-linear inverse modeling and global ocean state estimation. *Geoscientific Model Development*, *8*, 3071–3104. https://doi.org/10.5194/gmd-8-3071-2015

Forget, G., Ferreira, D., & Liang, X. (2015). On the observability of turbulent transport rates by Argo: Supporting evidence from an inversion experiment. *Ocean Science*, *11*(5), 839–853. https://doi.org/10.5194/os-11-839-2015

Fossheim, M., Primicerio, R., Johannesen, E., Ingvaldsen, R. B., Aschan, M. M., & Dolgov, A. V. (2015). Recent warming leads to a rapid borealization of fish communities in the Arctic. *Nature Climate Change*, *5*, 673–677. https://doi.org/10.1038/nclimate2647

Foukal, N. P., & Lozier, M. S. (2018). Examining the origins of ocean heat content variability in the eastern North Atlantic subpolar gyre. *Geophysical Research Letters*, *45*, 11,275–11,283. https://doi.org/10.1029/2018GL079122

Fukumori, I., Wang, O., Fenty, I., Forget, G., Heimbach, P., & Ponte, R. M. (2017). ECCO Version 4 Release 3.

Gent, P. R., & Mcwilliams, J. C. (1990). Isopycnal mixing in ocean circulation models. *Journal of Physical Oceanography*, *20*(1), 150–155. https://doi.org/10.1175/1520-0485(1990)020<0150:IMIOCM>2.0.CO;2

Hamed, K. H., & Rao, R. A. (1997). A modified Mann-Kendall trend test for autocorrelated data. *Journal of Hydrology*, *204*, 182–196. https://doi.org/10.1016/S0022-1694(97)00125-X

Heimbach, P., Hill, C., & Giering, R. (2005). An efficient exact adjoint of the parallel MIT General Circulation Model, generated via automatic differentiation. *Future Generation Computer Systems*, *21*(8), 1356–1371. https://doi.org/10.1016/J.FUTURE.2004.11.010

Kim, K.-Y., Kim, J.-Y., Kim, J., Yeo, S., Na, H., Hamlington, B. D., & Leben, R. R. (2019). Vertical feedback mechanism of winter Arctic amplification and sea ice loss. *Scientific Reports*, *9*, 1184. https://doi.org/10.1038/s41598-018-38109-x

Koenigk, T., & Brodeau, L. (2014). Ocean heat transport into the Arctic in the twentieth and twenty-first century in EC-Earth. *Climate Dynamics*, *42*, 3101–3120. https://doi.org/10.1007/s00382-013-1821-x

Kohnemann, S. H. E., Heinemann, G., Bromwich, D. H., & Gutjahr, O. (2017). Extreme warming in the Kara sea and Barents Sea during the winter period 2000-16. *Journal of Climate*, *30*(22), 8913–8927. https://doi.org/10.1175/JCLI-D-16-0693.1

Large, W., & Yeager, S. G. (2004). Diurnal to decadal global forcing for ocean and sea-ice models: The data sets and flux climatologies. https://doi.org/10.5065/D6KK98Q6

Lee, T., Fukumori, I., & Tang, B. (2004). Temperature advection: Internal versus external processes. *Journal of Physical Oceanography*, *34*(8), 1936–1944. https://doi.org/10.1175/1520-0485(2004)034<1936:TAIVEP>2.0.CO;2

Liang, X., Spall, M., & Wunsch, C. (2017). Global ocean vertical velocity from a dynamically consistent ocean state estimate. *Journal of Geophysical Research: Oceans*, *122*, 8208–8224. https://doi.org/10.1002/2017JC012985

Lind, S., Ingvaldsen, R. B., & Furevik, T. (2018). Arctic warming hotspot in the northern Barents Sea linked to declining sea-ice import. *Nature Climate Change*, *8*, 634–639. https://doi.org/10.1038/s41558-018-0205-y

Loeng, H. (1991). Features of the physical oceanographic conditions of the Barents Sea. *Polar Research*, *10*(1), 5–18. https://doi.org/10.3402/polar.v10i1.6723

Onarheim, I. H., & Årthun, M. (2017). Toward an ice-free Barents Sea. *Geophysical Research Letters*, *44*, 8387–8395. https://doi.org/10.1002/2017GL074304

Ottersen, G., Ådlandsvik, B., & Loeng, H. (2000). Predicting the temperature of the Barents Sea. *Fisheries Oceanography*, *9*(2), 121–135. https://doi.org/10.1046/j.1365-2419.2000.00127.x

Piecuch, C. G., Ponte, R. M., Little, C. M., Buckley, M. W., & Fukumori, I. (2017). Mechanisms underlying recent decadal changes in subpolar North Atlantic Ocean heat content. *Journal of Geophysical Research: Oceans*, *122*, 7181–7197. https://doi.org/10.1002/2017JC012845

Polyakov, I. V., Pnyushkov, A. V., Alkire, M. B., Ashik, I. M., Baumann, T. M., Carmack, E. C., et al. (2017). Greater role for Atlantic inflows on sea-ice loss in the Eurasian Basin of the Arctic Ocean. *Science*, *356*(6335), 285–291. https://doi.org/10.1126/science.aai8204

Sandø, A. B., Nilsen, J. E., Gao, Y., & Lohmann, K. (2010). Importance of heat transport and local air-sea heat fluxes for Barents Sea climate variability. *Journal of Geophysical Research*, *115*, C07013. https://doi.org/10.1029/2009JC005884

Schlichtholz, P. (2019). Subsurface ocean flywheel of coupled climate variability in the Barents Sea hotspot of global warming. *Scientific Reports*, *9*, 13,692. https://doi.org/10.1038/s41598-019-49965-6

Screen, J. A., Deser, C., Smith, D. M., Zhang, X., Blackport, R., Kushner, P. J., et al. (2018). Consistency and discrepancy in the atmospheric response to Arctic sea-ice loss across climate models. *Nature Geoscience*, *11*, 155–163. https://doi.org/10.1038/s41561-018-0059-y

Signorini, S. R., & McClain, C. R. (2009). Environmental factors controlling the Barents Sea spring-summer phytoplankton blooms. *Geophysical Research Letters*, *36*, L10604. https://doi.org/10.1029/2009GL037695

Skagseth, Ø, Eldevik, T., Årthun, M., Asbjørnsen, H., Lien, V. S., & Smedsrud, L. H. (2020). Reduced efficiency of the Barents Sea cooling machine. *Nature Climate Change*, *10*, 661–666. https://doi.org/10.1038/s41558-020-0772-6

Smedsrud, L. H., Esau, I., Ingvaldsen, R. B., Eldevik, T., Haugan, P. M., Li, C., et al. (2013). The role of the Barents Sea in the Arctic climate system. *Reviews of Geophysics*, *51*, 415–449. https://doi.org/10.1175/JCLI-D-15-0046.1

Smedsrud, L. H., Ingvaldsen, R., Nilsen, J. E., & Skagseth, O. (2010). Heat in the Barents Sea: Transport, storage, and surface fluxes. *Ocean Science*, *6*, 219–234. https://doi.org/10.5194/os-6-219-2010

Sorokina, S. A., Li, C., Wettstein, J. J., & Kvamstø, N. G. (2016). Observed atmospheric coupling between Barents Sea ice and the warm-Arctic cold-Siberian anomaly pattern. *Journal of Climate*, *29*, 495–511. https://doi.org/10.1029/2019GL083837

Wang, Q., Wang, X., Wekerle, C., Danilov, S., Jung, T., Koldunov, N., et al. (2019). Ocean heat transport into the Barents Sea: Distinct controls on the upward trend and interannual variability. *Geophysical Research Letters*, *46*, 13,180–13,190. https://doi.org/10.1029/2019GL083837

Woods, C., & Caballero, R. (2016). The role of moist intrusions in winter Arctic warming and sea ice decline. *Journal of Climate*, *29*(12), 4473–4485. https://doi.org/10.1175/JCLI-D-15-0773.1